



Published in Image Processing On Line on 2021-12-19.
Submitted on 2021-12-03, accepted on 2021-12-18.
ISSN 2105-1232 © 2021 IPOL & the authors CC-BY-NC-SA
This article is available online with supplementary materials,
software, datasets and online demo at
<https://doi.org/10.5201/ipol.2021.391>

Center/Surround Retinex: Analysis and Implementation

Jose-Luis Lisani, Ana-Belén Petro, Catalina Sbert

Universitat Illes Balears, Spain

{jose-luis.lisani, anabelen.petro, catalina.sbert}@uib.es

Communicated by Jean-Michel Morel *Demo edited by* Jose-Luis Lisani

Abstract

The Retinex perception theory tries to mimic the human ability to cope with the high dynamic range of natural scenes. In 1986 E. Land proposed a formulation of this model in terms of a Center/Surround operation involving two steps, a local adaptation and a global transform. This model gave rise to the so-called Center/Surround tone-mapping algorithms. In this paper we unify the different Center/Surround algorithms proposed in the literature using a common framework and analyze several possibilities for the local and global operations involved.

Source Code

The reviewed and documented source code and an online demo are available at [the web page of this article](#)¹. Compilation and usage instructions are included in the README.txt file of the archive.

Keywords: Retinex theory; tone mapping; center/surround method; color enhancement

1 Introduction

The adaptation of the human visual system (HVS) to several orders of magnitude of light intensity permits us to perceive a wide spectrum of lights and contrasts which, in general, a camera is unable to capture. The reason is that the eye is a contrast detector, not an absolute detector like the sensor in a digital camera. Edwin Land proposed, in 1964, a complex algorithm involving image paths to compute relative lightness values from the absolute values captured by the camera [6].

Later, he published [7] an alternative formulation of the original algorithm in which the relative lightness was computed as the ratio between the value of a pixel and the weighted average of the surrounding values. This operation was followed by a logarithmic mapping of the ratios in order to mimic the non-linear behaviour of the HVS with respect to low and high values of the illumination.

¹<https://doi.org/10.5201/ipol.2021.391>

A generalization of this formulation leads to the following model for the computation of the image lightness L

$$L(\mathbf{x}) = f\left(\frac{I(\mathbf{x})}{F * I(\mathbf{x})}\right), \tag{1}$$

where $I(x)$ is the light intensity captured by the camera at pixel \mathbf{x} (we are considering here a single-channel image), F is a surround radial kernel, and f is a global scaling function.

Equation (1) defines a **Center/Surround model** of image perception. In this paper we shall analyze different alternatives both for the kernel and the scaling function, and we will give algorithmical details of the implementation of the model. For a more detailed analysis we refer the reader to [10].

The paper is organized as follows: in Section 2 different alternatives for the kernel function are analyzed; similarly, several possible scaling functions are examined in Section 3. The main center/surround algorithm is described in Section 4, together with some technical details. Several experiments are displayed in Section 5, and some conclusions are drawn in Section 6.

2 Kernel Functions

Mathematically, two conditions should be imposed to the kernel: scale invariance and integrability. As proved in [14], the only radial kernel which is scale invariant is $F(r) = \frac{K}{r^2}$, which is the (non-integrable) kernel proposed by Land in [7]. Several other radial kernels have been proposed in the literature [7, 13, 5, 4, 3, 12, 14, 17]. In [10] an exhaustive analysis of these kernels is performed, and some new ones are proposed. The authors unify all these kernels into five models, which are summarized in Table 1 and described next:

- F_{AG} is the generalization of the Gaussian kernel and a linearized version of the multiscale Retinex (MSR) [4]. It is a weighted average of Gaussian kernels at different scales and it is defined as

$$F_{AG}(r) = \sum_{i=1}^N w_i F_{G,\sigma_i} = \sum_{i=1}^N w_i \frac{1}{2\pi\sigma_i^2} e^{-\frac{r^2}{2\sigma_i^2}}, \tag{2}$$

where N is the number of scales, σ_i is the scale parameter of the i -th kernel and w_i is its corresponding weight factor.

Following [4], the scales are distributed following a geometric series

$$\sigma_i = \sigma_1 r^{i-1}.$$

The initial scale σ_1 is a parameter. Since convolutions with Gaussians whose σ is of the order of the image size or bigger yield a constant result, the final scale σ_N can be chosen depending on the image dimensions

$$\sigma_N = S \cdot \min(\text{image width}, \text{image height}),$$

where S is also a parameter.

Finally, we propose to define the weights as $w_i = \frac{1}{N}$. In this way, we have reduced the parameters of the kernel to N , σ_1 and S .

- F_{IG} was first introduced in [14] to find a compromise between scale invariance and integrability. It is a continuous average of Gaussians from scale σ_1 to σ_2 .

$$F_{IG}(r) = \begin{cases} \frac{1}{2\pi \log(\sigma_2/\sigma_1)} \frac{\exp\left(-\frac{r^2}{2\sigma_2^2}\right) - \exp\left(-\frac{r^2}{2\sigma_1^2}\right)}{r^2}, & r \neq 0, \\ \frac{\sigma_1^{-2} - \sigma_2^{-2}}{4\pi \log(\sigma_2/\sigma_1)}, & r = 0. \end{cases} \quad (3)$$

where the initial scale σ_1 is a parameter, and the final scale σ_2 is chosen depending on the image size as in the previous case

$$\sigma_N = S \cdot \min(\text{image width}, \text{image height}),$$

where S is also a parameter.

- $F_{2,\sigma}$ is the continuous version of the Land kernel $F(r) = 1/r^2$

$$F_{2,\sigma}(r) = \frac{C}{\left(\frac{r}{\sigma}\right)^2 + 1}, \quad (4)$$

where C is a normalization constant such that $\int_{\Omega} F_{2,\sigma}(r) dr = 1$.

- F_{IE} is a continuous average of exponentials

$$F_{IE}(r) = \begin{cases} \frac{1}{2\pi(\sigma_2 - \sigma_1)} \frac{e^{-\frac{r}{\sigma_2}} - e^{-\frac{r}{\sigma_1}}}{r} & r \neq 0, \\ \frac{1}{2\pi\sigma_2\sigma_1} & r = 0. \end{cases} \quad (5)$$

It is inspired by an early work by Moore et al. [13], which proposed an exponential kernel

$$F_{E,\sigma}(r) = \frac{1}{2\pi\sigma^2} e^{-\frac{r}{\sigma}}, \quad (6)$$

that permitted a real-time implementation in analog VLSI.

In F_{IE} the weight of the central point in the convolution kernel is of order $\mathcal{O}\left(\frac{1}{\sigma_1\sigma_2}\right)$ showing the inverse proportionality of both parameters. As is analyzed in [10], to obtain good results the product between σ_1 and σ_2 must be constant. Since the kernel is not scale invariant, the values of the initial and final scales σ_1 and σ_2 are chosen depending on the image size as

$$\sigma_1 = s / \min(\text{image width}, \text{image height}),$$

$$\sigma_2 = S \cdot \min(\text{image width}, \text{image height}),$$

where s and S are parameters.

- $F_{1,\sigma}$ is the continuous version of the ACE kernel [17]

$$F_{1,\sigma}(r) = \frac{C}{\left(\frac{r}{\sigma}\right) + 1}, \quad (7)$$

where C is a normalization constant such that $\int_{\Omega} F_{1,\sigma}(r)dr = 1$.

This kernel is not scale invariant, therefore the scale σ is chosen depending on the image size as

$$\sigma = s/\min(\text{image width, image height}),$$

where s is a parameter.

| Kernel | Parameters |
|--|--|
| $F_{AG}(r) = \sum_{i=1}^N w_i F_{G,\sigma_i}$ | N, σ_1, S $\sigma_N = S \cdot \min. \text{ image dimension}$ $\sigma_i = \sigma_1 \left(\frac{\sigma_N}{\sigma_1} \right)^{\frac{i-1}{N-1}}$ $w_i = \frac{1}{N}$ $i = 1, \dots, N$ |
| $F_{IG}(r) = \begin{cases} C \frac{\exp\left(\frac{-r^2}{2\sigma_2^2}\right) - \exp\left(\frac{-r^2}{2\sigma_1^2}\right)}{r^2}, & r \neq 0 \\ C \frac{\sigma_1^{-2} - \sigma_2^{-2}}{2} & r = 0 \end{cases}$ | σ_1, S $\sigma_2 = S \cdot \min. \text{ image dimension}$ |
| $C = \frac{1}{2\pi \log(\sigma_2/\sigma_1)}$ | |
| $F_{IE}(r) = \begin{cases} C \frac{\exp\left(\frac{-r}{\sigma_2}\right) - \exp\left(\frac{-r}{\sigma_1}\right)}{r}, & r \neq 0 \\ \frac{1}{2\pi\sigma_2\sigma_1}, & r = 0 \end{cases}$ | s, S $\sigma_1 = s/\min. \text{ image dimension}$ $\sigma_2 = S \cdot \min. \text{ image dimension}$ |
| $C = \frac{1}{2\pi(\sigma_2 - \sigma_1)}$ | |
| $F_{1,\sigma}(r) = \frac{C}{\left(\frac{r}{\sigma}\right) + 1}$ | s $\sigma = s/\min. \text{ image dimension}$ |
| $F_{2,\sigma}(r) = \frac{C}{\left(\frac{r}{\sigma}\right)^2 + 1}$ | σ |

Table 1: The five models of surround kernels that summarize the state of the art.

Optimum Values of the Kernel Parameters

In [10] the authors studied, in terms of some distortion measures, the range of values of the parameters of the different kernels. In this study they observed that kernels F_{AG} , F_{IG} and $F_{2,\sigma}$, which are differentiable at $r = 0$, produce more halo distortion than F_{IE} and $F_{1,\sigma}$ which are non-differentiable at $r = 0$. This is because the halo becomes more visible as the size of the kernel decreases, and the non-differentiable kernels have a less local behavior. Table 2 presents the recommended parameter values. In Section 5 several examples illustrate how these parameters influence the obtained results.

| Kernel | Recommended parameter values |
|----------------|---|
| F_{AG} | $N = 5, S \geq 0.5, \sigma_1$ indifferent |
| F_{IG} | $S \geq 1, \sigma_1 \geq 0.25$ |
| F_{IE} | $S \geq 0.5, s \geq 0.5$ |
| $F_{2,\sigma}$ | $\sigma \geq 0.25$ |
| $F_{1,\sigma}$ | $s \geq 0.1$ |

Table 2: Recommended ranges of values of the parameters of the kernels that guarantee a minimum degree of visual distortion in the results.

3 Scaling Functions

The human visual system (HVS) is able to discount the effect of the illumination in the perception of the scenes. The Retinex theory tries to mimic the HVS, with the center/surround formulation. Moreover, Land in [8] observed that the function which relates reflectance with lightness sensation can be approximated by a logarithmic function. Naka and Rushton [15] were the first to model the contrast sensitivity as a sigmoid function. Reinhard in [16] noticed the mathematical properties of sigmoid functions to model the HVS. On the other hand digital images suffer several camera processes, such as gamma-corrections and white balance, which these mapping functions must take into account. In [10] different options for these mapping functions (also known as scaling functions) were analyzed. Table 3 summarizes them. Note that these functions are defined for single channel images. For color images they are applied on a channel-by-channel basis.

In what follows, Min and Max refer to the minimum and maximum values of the range of the center/surround operation $\frac{I}{F * I}$, which shall be mapped to the usual $[0, 255]$ range.

| Name | Function f |
|-----------------|---|
| Linear | $f_L(x) = 255 \left(\frac{x - Min}{Max - Min} \right)$ |
| Logarithmic | $f_{log}(x) = \frac{255}{\log(Max - Min + 1)} \log(x - Min + 1)$ |
| Power | $f_\alpha(x) = 255 \left(\frac{x - Min}{Max - Min} \right)^\alpha$ |
| Naka-Rushton | $f_{NR}(x) = \frac{255(A+1)(x - Min)}{A(Max - Min) + x - Min}$ |
| Histogram based | $f_E(x) = C \int_{Min}^x h(t)^{\frac{1}{p+1}} dt$ |

Table 3: Scaling functions reviewed in Section 3.

- Linear mapping. It consists in just a linear stretching of the input range to the desired output range.

$$f_L(x) = 255 \left(\frac{x - Min}{Max - Min} \right). \quad (8)$$

- Logarithmic mapping. Inspired by the tone curve proposed by Drago et al. [1], which produces better results (less noisy in dark areas) than simply replacing the linear values by logarithms in Equation (8).

$$f_{log}(x) = \frac{255}{\log(Max - Min + 1)} \log(x - Min + 1). \quad (9)$$

- Power function.

$$f_\alpha(x) = 255 \left(\frac{x - Min}{Max - Min} \right)^\alpha \quad (10)$$

The parameter α can take positive and negative values. In our implementation, we have the option to automatically fix α so that the median of the input values is mapped to the center of the output range, i.e. 127.5^2 .

- Naka-Rushton function. Naka and Rushton [15] modeled the contrast sensitivity in the human visual system as the sigmoid function $f(x) = \frac{x}{x+s}$, where s is the value which is mapped to 0.5. We modify this function such that Min is mapped to 0 and Max is mapped to 255.

$$f_{NR}(x) = \frac{255(A+1)(x - Min)}{A(Max - Min) + x - Min}, \quad (11)$$

where $A > 0$ is a constant that controls the steepness of the function. For large values of A f_{NR} tends to a linear function f_L .

In our implementation, we have the option to automatically fix A so that the median of the input values is mapped to the center of the output range, i.e. 127.5^3 . Note that this can only be achieved for positive values of A when the median is below $\frac{Min+Max}{2}$. If this is not the case, A is fixed automatically to a large value, so f_{NR} becomes linear.

- Taking into account the shape of the histogram of the center/surround operation $\frac{I}{F * I}$, we consider a histogram-based function, which is adapted to the pixel distribution of the values. It is a generalization of the one proposed by Mai et al. [11]. The function is computed as the minimizer of the functional

$$\min_g \int_{Min}^{Max} \frac{h(x)}{g'(x)^p} dx,$$

subject to the condition

$$\int_{Min}^{Max} g'(x) dx = 255,$$

where h denotes the normalized histogram and $p > 0$ is a parameter.

The closed-form solution of the minimizing problem is

$$f_E(x) = C \int_{Min}^x h(t)^{\frac{1}{p+1}} dt. \quad (12)$$

where C is such that $f_E(Max) = 255$. Observe that for $p = 0$ f_E is a histogram equalization. In general, the parameter is fixed to $p = 2$, as proposed in [11].

²In our implementation, if the automatically computed α is smaller than 0.3, then its value is clipped to 0.3, to prevent excessive enhancement of low input values.

³In our implementation, if the automatically computed A is smaller than 0.1, then its value is clipped to 0.1, to prevent excessive enhancement of low input values.

Definition of *Min* and *Max*. The values defining the range of the center/surround operation $\frac{I}{F * I}$ could simply be computed as the minimum and maximum values of this operation. However, in order to increase the dynamic range of the final output, it is sometimes useful to clip to either 0 (black) or 255 (white) some of the lowest (resp. highest) values of the original range. Therefore, *Min* and *Max* are computed by selecting the percentages of image pixels that will be clipped to black ($s_{\text{black}}\%$) or white ($s_{\text{white}}\%$). Algorithm 1 describes how these values are computed. This algorithm is an adaptation of the algorithm for robust normalization proposed in [2], which itself is a variant of the simplest color balance algorithm proposed in [9].

Algorithm 1: Compute Min-Max (adapted from [2])

```

Input      : input image  $u$  with  $N$  pixels
Input      : percentage of saturation in the white and the black, respectively  $s_{\text{white}}$  and  $s_{\text{black}}$ 
Output    : Min, Max
1 if  $u$  is color image then
2   |  $u_{\text{max}} \leftarrow \max\{u_R, u_G, u_B\}$  //Compute max channel
3   |  $u_{\text{min}} \leftarrow \min\{u_R, u_G, u_B\}$  //Compute min channel
4 else
5   |  $u_{\text{max}} \leftarrow u$ 
6   |  $u_{\text{min}} \leftarrow u$ 
7  $\bar{u}_{\text{max}} \leftarrow \text{Sort}(u_{\text{max}})$  //Sort increasing
8  $\bar{u}_{\text{min}} \leftarrow \text{Sort}(u_{\text{min}})$  //Sort increasing
9  $\text{Min} \leftarrow \bar{u}_{\text{min}}(\lfloor \frac{s_{\text{black}}}{100} N \rfloor)$  //Find minimum value
10  $\text{Max} \leftarrow \bar{u}_{\text{max}}(\lceil (1 - \frac{s_{\text{white}}}{100}) N - 1 \rceil)$  //Find maximum value

```

4 Center/Surround Algorithm

The complete algorithm for the computation of the center/surround operation on an image is presented in Algorithm 2.

Computation of the convolution $I * F$. The convolution between the original image and the kernel function is computed in the Fourier domain. By using the FFT and IFFT functions of the FFTW software library⁴ the original image is extended symmetrically across its sides, so that the extended image, which is four times bigger, becomes symmetric and periodic. In fact, with the FFTW library the symmetrization is implicit and performed directly as a cosine transform. By using these functions the convolution is computed as

$$I * F = \text{IFFT}\{\text{DFT}(I) \cdot \text{DFT}(F)\}.$$

5 Experiments

In a previous article [10], we carried out an analysis for different combinations of kernel and global mappings, using quantitative and qualitative criteria, over HDR images. For these images, most of the values were concentrated on the lower part of their dynamic range. This is not usually the case for the LDR images studied in the current paper. For this reason the conclusions of our analysis

⁴M. Frigo and S. G. Johnson. FFTW package. <http://www.fftw.org/>

Algorithm 2: Center/Surround Retinex Algorithm

```

Input      : input image  $u$ 
Output    : processed image  $v$ 
Parameters: kernel type  $F \in \{F_{AG}, F_{IG}, F_{IE}, F_1, F_2\}$  scaling function
                $f \in \{f_L, f_{log}, f_\alpha, f_{NR}, f_E\}$ , percentages of black and white saturated pixels ( $s_{black}$ 
               and  $s_{white}$ ), parameters of kernels and scaling functions

1 for each image channel  $I$  from  $u$  do
    //Compute  $I' = I * F$ 
2   if  $F == F_{AG}$  then
    //Compute weighted sum of Gaussian convolutions
3      $I' \leftarrow 0$ 
4     for each  $i \in \{1, \dots, N\}$  do
5        $I' \leftarrow I' + w_i \cdot I * F_{G, \sigma_i}$ 
6   else
    //Compute convolution
7      $I' \leftarrow I * F$ 
    //Compute center/surround image
8    $I_{CS} = \frac{I}{I + \epsilon}$  //Add small constant value ( $\epsilon = 10^{-8}$ ) to avoid division by zero
    //Compute range  $[Min, Max]$ 
9    $Min, Max \leftarrow \text{Compute\_Min\_Max}(u, s_1, s_2)$  //Algorithm 1
    //Map range  $[Min, Max]$  to  $[0, 255]$  using scaling function  $f$ 
10   $v \leftarrow \emptyset$  //Initialize output image
11 for each image channel  $I_{CS}$  do
12    $I_{out} \leftarrow f(I_{CS})$ 
13    $v \leftarrow v \cup I_{out}$  //Add processed channel to output image
14 return  $v$ 
    
```

are slightly different from the ones in [10]. In general, we have observed that, for these images, the recommended ranges of values of the parameters of the kernels, shown in Table 2, are correct, but some minimum values must be increased.

In Figure 1 we compare the value of different parameters for the F_{AG} kernel, with a fixed scaling function (f_{log}). In this image, we can observe that we obtain better results with the number of scales greater or equal to 5. We also observe that values of S smaller than 0.5 produce artifacts in the image. The tests show that the variation of the σ_1 parameter does not produce meaningful changes in the results.

In the case of the F_{IG} kernel, the minimum recommended value of the σ_1 parameter in Table 2 is 0.125, however, for most LDR images it produces excessively bright results. A value greater or equal to 0.5 produces better results in this case. This fact can be observed in Figure 2.

The recommended values for the parameters of the kernel F_{IE} in Table 2 are valid for the tested LDR images. However, the parameter of the kernel $F_{1, \sigma}$ must be increased. In Figure 3, we can observe that values smaller than 0.5 may enhance excessively the bright parts of the image.

Finally, the σ parameter for the kernel $F_{2, \sigma}$ should be set to values greater than 0.5, as it can be seen in the experiments of Figure 4.

In Figure 5, we can compare the results obtained with the different kernels on the same input image and with a fixed scaling function (f_{log}). The parameters of the kernels are fixed to their optimum values according to the previous comments. We observe that the non-differentiable kernels,



Calobra image



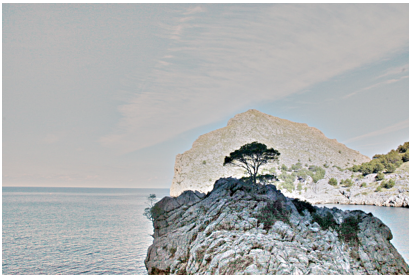
$N = 2, \sigma_1 = 0.5, S = 1$



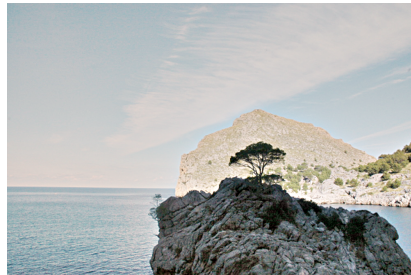
$N = 5, \sigma_1 = 0.5, S = 1$



$N = 10, \sigma_1 = 0.5, S = 1$



$N = 5, \sigma_1 = 1, S = 0.125$



$N = 5, \sigma_1 = 1, S = 0.5$

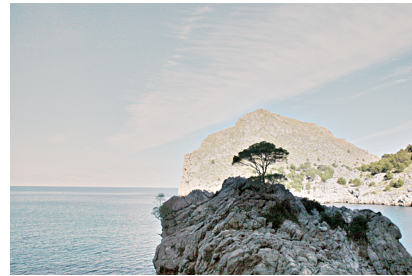


$N = 5, \sigma_1 = 1, S = 2$

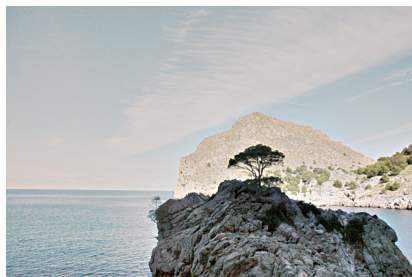
Figure 1: Comparison between the different parameters with the F_{AG} kernel with f_{log} scaling function.



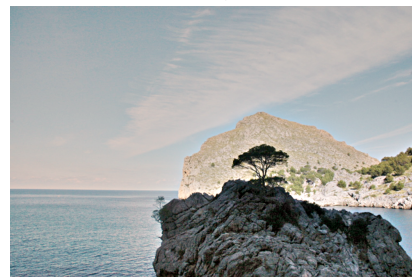
$\sigma_1 = 0.125, S = 1$



$\sigma_1 = 0.5, S = 1$



$\sigma_1 = 1, S = 1$



$\sigma_1 = 4, S = 1$

Figure 2: Comparison between the different parameters with the F_{IG} kernel with f_{log} scaling function applied to the image *Calobra* in Figure 1.



Figure 3: Comparison between the different parameters with the $F_{1,\sigma}$ kernel with f_{log} scaling function applied to the image *Calobra* in Figure 1.



Figure 4: Comparison between the different parameters with the $F_{2,\sigma}$ kernel with the f_{log} scaling function applied to the image *Calobra* in Figure 1.

F_{IE} and $F_{1,\sigma}$, obtain much better results, in terms of creation of halo artifacts. This is because the halo becomes more visible as the size of the kernel decreases, and the non-differentiable kernels have a less local behavior than the differentiable ones. Finally, in Figure 6, we can see another example. In this case, the halo artifacts are not detectable, but we can observe an excessive saturation in the window when using non-differentiable kernels.

If we analyze the scaling functions and their parameters, we observe that most of them have no parameters, or these can be fixed automatically to obtain that the median of the values of the C/S output is mapped to 127.5. Some results obtained with different values of the parameters for

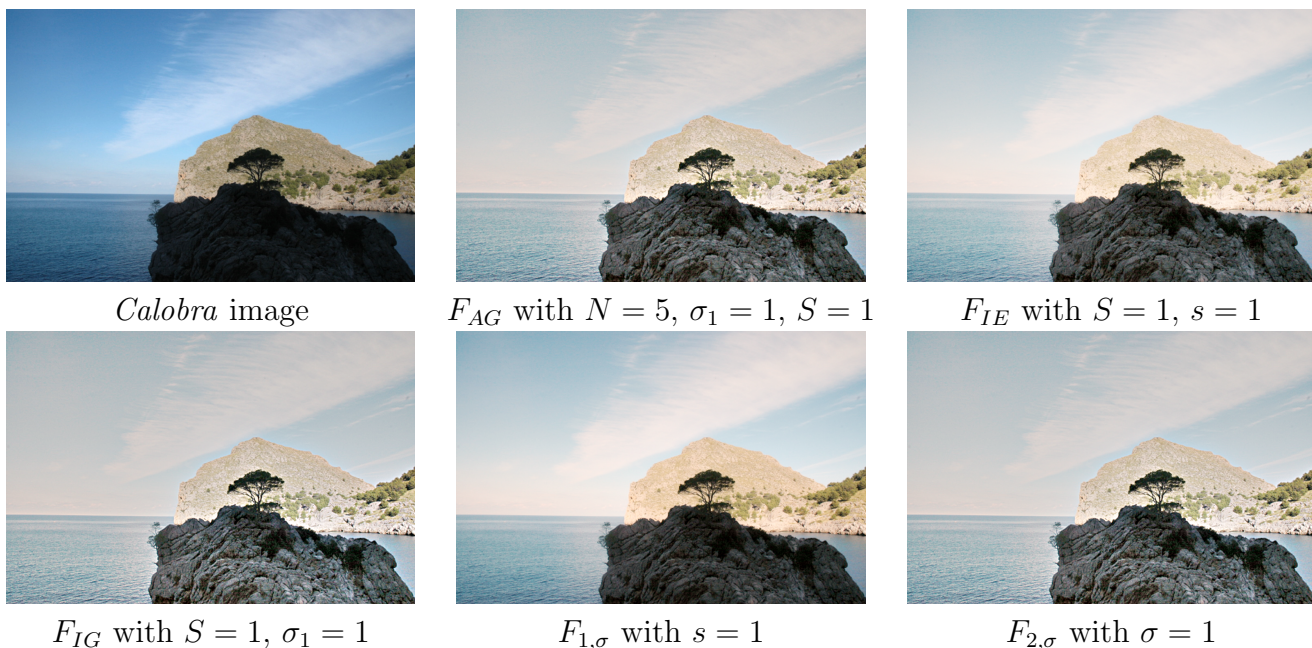


Figure 5: Comparison between the different kernels with the f_{log} scaling function.

functions f_α and f_{NR} are displayed in Figure 7.

Figures 8, 9 and 10 show results obtained with the different scaling functions (using the automatically estimated parameters when necessary) and three different kernels. In general, the results are brighter for f_{log} and f_{NR} , and better contrasted for f_E . In some images (e.g. Figure 9) the results with the f_α scaling are excessively dark.

6 Conclusions

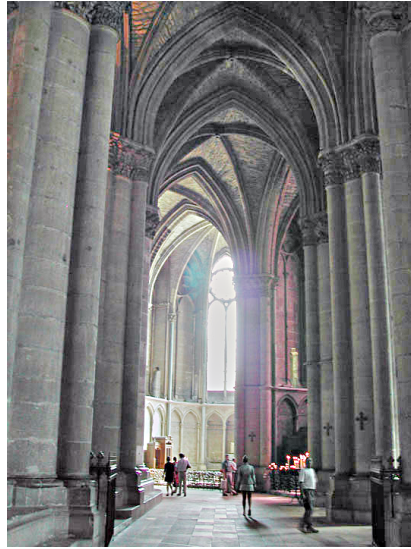
The center/surround formulation of the Retinex theory has been thoroughly analyzed in this paper. Several alternatives, both for kernel and scaling functions, have been considered.

Experiments conducted on several images show that non-differentiable kernels at $r = 0$ (F_{IE} , $F_{1,\sigma}$), being less local, produce fewer visual artifacts (e.g. halos) than differentiable ones (F_{AG} , F_{IG} , $F_{2,\sigma}$). On the other hand, the rendition of image details is better for the latter. Regarding the scaling functions, f_E produces the better contrasted results.

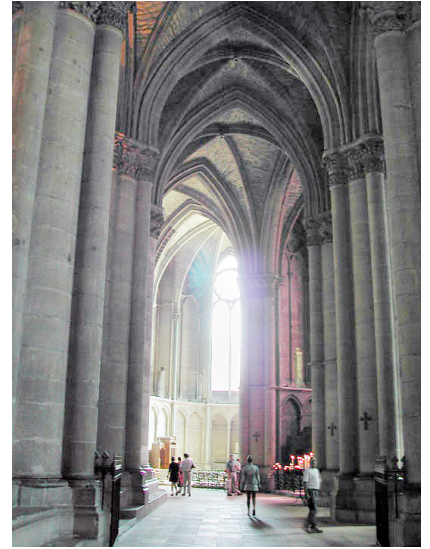
The reader is invited to test the different options with the online demo associated to the article.



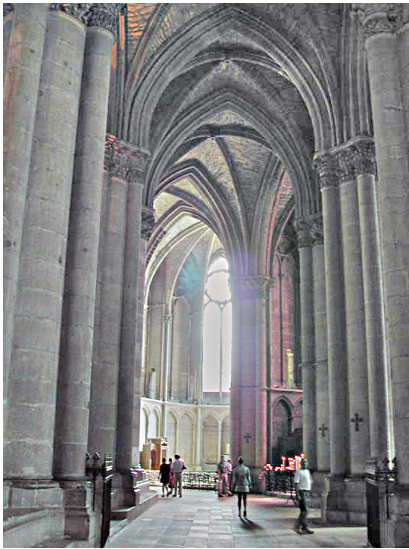
Cathedral image



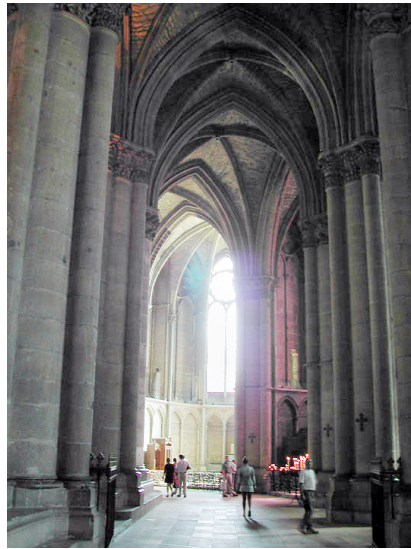
F_{AG} with $N = 5, \sigma_1 = 1, S = 1$



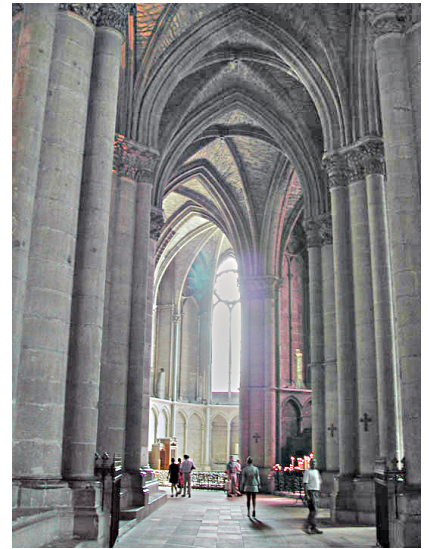
F_{IE} with $S = 1, s = 1$



F_{IG} with $S = 1, \sigma_1 = 1$



$F_{1,\sigma}$ with $s = 1$



$F_{2,\sigma}$ with $\sigma = 1$

Figure 6: Comparison between the different kernels with f_{log} scaling function.



Swam image



f_α with automatic value



f_α with $\alpha = 0.5$



f_α with $\alpha = 2$



f_{NR} with automatic value



f_{NR} with $A = 2$



f_{NR} with $A = 4$

Figure 7: Comparison between the results obtained with different parameters for the f_α and f_{NR} scaling functions, with fixed F_{IG} kernel.

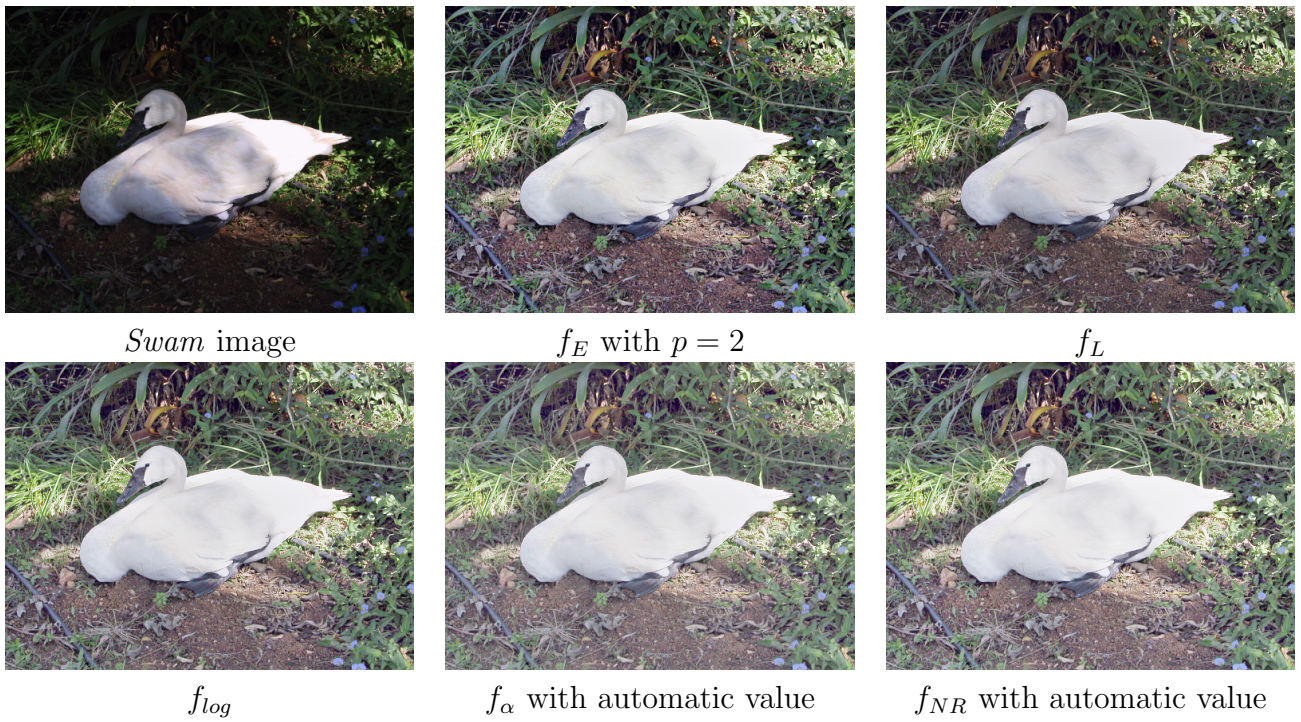


Figure 8: Comparison between the results obtained with different scaling functions, using a fixed F_{IE} kernel.

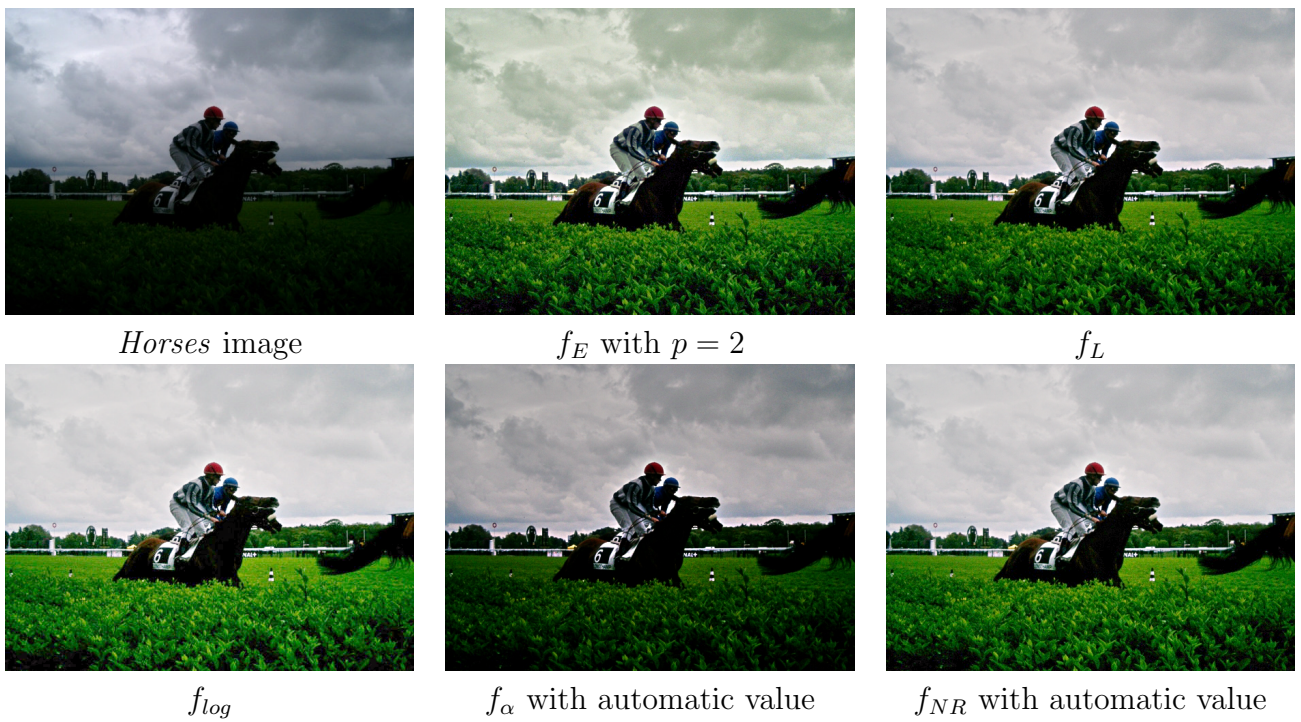


Figure 9: Comparison between the results obtained with different scaling functions, using a fixed F_{AG} kernel.



Horses image



f_E with $p = 2$



f_L



f_{log}



f_α with automatic value



f_{NR} with automatic value

Figure 10: Comparison between the results obtained with different scaling functions, using a fixed $F_{1,\sigma}$ kernel.

Acknowledgements

The authors have been partially sponsored by MINECO/AEI/FEDER, UE projects TIN2017-85572-P, DPI2017-86372-C3-3-R, and by the Comunitat Autònoma de les Illes Balears through the Direcció General de Política Universitària i Recerca with funds from the Tourist Stay Tax Law ITS 2017-006 (PRD2018/26).

Image Credits



A.B. Petro CC-BY.



NASA



Unknown author.

References

- [1] F. DRAGO, K. MYZKOWSKI, T. ANNEN, AND N. CHIBA, *Adaptive logarithmic mapping for displaying high contrast scenes*, Computer Graphics Forum, 22 (2003), pp. 419–426. <http://dx.doi.org/10.1111/1467-8659.00689>.
- [2] C. HESSEL, *An Implementation of the Exposure Fusion Algorithm*, Image Processing On Line, 8 (2018), pp. 369–387. <https://doi.org/10.5201/ipol.2018.230>.
- [3] A.C. HULBERT, *Formal connections between lightness algorithms*, Journal of the Optical Society of America, 3 (1986), pp. 1684–1693. <https://doi.org/10.1364/JOSAA.3.001684>.
- [4] D.J. JOBSON, Z. RAHMAN, AND G.A. WOODSELL, *A multiscale retinex for bridging the gap between color images and the human observation of scenes*, IEEE Transactions on Image Processing, 6 (1997), pp. 965–976. <https://doi.org/10.1109/83.597272>.
- [5] D.J. JOBSON, Z. RAHMAN, AND G.A. WOODSELL, *Properties and performance of a center/surround retinex*, IEEE Transactions on Image Processing, 6 (1997), pp. 451–462. <https://doi.org/10.1109/83.557356>.
- [6] E.H. LAND, *The retinex*, American Scientist, 52 (1964), pp. 247–264.
- [7] E.H. LAND, *An alternative technique for the computation of the designator in the retinex theory of color vision*, in Proceedings of the National Academy of Science, vol. 83 of 10, 1986, pp. 3078–3080. <https://dx.doi.org/10.1073/pnas.83.10.3078>.
- [8] E. H. LAND, *The retinex theory of color vision*, Scientific American, 237 (1977), pp. 108–128.
- [9] N. LIMARE, J.L. LISANI, J-M. MOREL, A.B. PETRO, AND C. SBERT, *Simplest Color Balance*, Image Processing On Line, 1 (2011), pp. 297–315. <https://doi.org/10.5201/ipol.2011.11mps-scb>.
- [10] J.L. LISANI, J-M. MOREL, A.B. PETRO, AND C. SBERT, *Analyzing center/surround retinex*, Information Sciences, 512 (2020), pp. 741–759. <https://doi.org/10.1016/j.ins.2019.10.009>.

- [11] Z. MAI, H. MANSOUR, R. MANTIUK, P. NASIOPOULOS, R. K. WARD, AND W. HEIDRICH, *Optimizing a tone curve for backward-compatible high dynamic range image and video compression*, IEEE Transactions on Image Processing, 20 (2011), pp. 1558–1571. <http://dx.doi.org/10.1109/TIP.2010.2095866>.
- [12] L. MEYLAN AND S. SÜSTRUNK, *Bio-inspired color image enhancement*, in SPIE, vol. 5292, 2004, pp. 46–56. <http://dx.doi.org/10.1117/12.526545>.
- [13] A. MOORE, J. ALLMAN, AND R. M. GOODMAN, *A real-time neural system for color constancy*, IEEE Transactions on Neural Networks, 2 (1991), pp. 237–246. <https://doi.org/10.1109/72.80334>.
- [14] J. M. MOREL, A. B. PETRO, AND C. SBERT, *What is the right center/surround for Retinex?*, in IEEE International Conference on Image Processing (ICIP), 2014, pp. 4552–4556. <https://doi.org/10.1109/ICIP.2014.7025923>.
- [15] K. I. NAKA AND W. A. H. RUSHTON, *S-potentials from colour units in the retina of fish (cyprinidae)*, Journal of Physiology, 185 (1966), pp. 536–555. <https://dx.doi.org/10.1113/jphysiol.1966.sp008001>.
- [16] E. REINHARD, G. WARD, S. PATTANAİK, AND P. DEBEVEC, *High Dynamic Range Imaging: Acquisition, Display, and Image-Based Lighting (The Morgan Kaufmann Series in Computer Graphics)*, Morgan Kaufmann Publishers Inc., San Francisco, CA, USA, 2005. ISBN 0125852630.
- [17] A. RIZZI, C. GATTA, AND D. MARINI, *A new algorithm for unsupervised global and local color correction*, Pattern Recognition Letters, 24 (2003), pp. 1663–1677. [https://doi.org/10.1016/S0167-8655\(02\)00323-9](https://doi.org/10.1016/S0167-8655(02)00323-9).